Wiley
International Journal of Antennas and Propagation
Volume 2024, Article ID 3826899, 14 pages
https://doi.org/10.1155/ijap/3826899

WILEY

Research Article

Self-Decoupled Quad-Port CPW-Fed Fractal MIMO Antenna With UWB Characteristics

Mian Muhammad Kamal,[1] **Binghao Wang**,[1] **Nosherwan Shoaib**,[2] **Umair Rafique**,[3] **Muhammad Inam Abbasi**,[4] **and Muhammad Ramlee Kamarudin**[5]

[1]*School of Electronic Science and Engineering, Southeast University, No. 2 Southeast University Road, Jiangning, Nanjing, Jiangsu 211189, China*
[2]*School of Electrical Engineering and Computer Science (SEECS), National University of Sciences and Technology (NUST), Islamabad 44000, Pakistan*
[3]*Centre for Wireless Communications, Faculty of Information Technology and Electrical Engineering, University of Oulu, Oulu 90570, Finland*
[4]*Faculty of Electrical and Electronic Engineering Technology, Universiti Teknikal Malaysia Melaka, Durian Tunggal 76100, Malaysia*
[5]*Faculty of Electrical and Electronic Engineering, Universiti Tun Hussein Onn Malaysia, Batu Pahat 86400, Malaysia*

Correspondence should be addressed to Binghao Wang; binghaowang@seu.edu.cn and Muhammad Ramlee Kamarudin; mramlee@uthm.edu.my

Received 3 September 2024; Accepted 18 November 2024

Academic Editor: Trushit Upadhyaya

In this work, a novel fractal multiple-input multiple-output (MIMO) antenna is designed for ultrawideband (UWB) applications. The radiating structure of the MIMO configuration employs a circular fractalradiating structure excited through a modified coplanar waveguide (CPW) feed. The fractal shape is designed by employing small circular rings inside the main circular ring patch element, which led to enhanced impedance bandwidth spanning from 3.15 to 20 GHz with acceptable radiation properties. The results show that the designed antenna has a peak gain of 6.13 dBi and radiation efficiency of > 85% in the operating bandwidth. Moreover, the single-antenna element exhibits stable radiation patterns in the UWB frequency spectrum. For MIMO communication systems, a polarization diversity-based quad-port MIMO antenna is designed. From the designed MIMO antenna configuration, an isolation of > 15 dB is achieved among the radiating elements without the use of any isolation enhancement network. Furthermore, MIMO performance parameters such as envelope correlation coefficient (ECC) of < 0.008, mean effective gain (MEG) of < −3 dB, channel capacity loss (CCL) of < 0.25 bps/Hz, and total active reflection coefficient (TARC) of > 20 dB are obtained from the proposed UWB MIMO antenna.

Keywords: fractal antenna; MIMO; polarization diversity; UWB

1. Introduction

Recent developments in wireless communication demand a system that has the ability to share vast amounts of data at a fast rate while maintaining low complexity [1]. These requirements can be achieved with the use of ultrawideband (UWB) technology because it has the capability to accommodate the transmission of high data rates with low-cost infrastructure. However, traditional UWB technology faces challenges with multipath propagation. To overcome this issue, one of the solutions is to employ multiple-input multiple-output (MIMO) antennas. Designing such antennas is challenging due to the additional performance characteristics that need to be considered, such as isolation among antenna elements to prevent channel capacity loss (CCL). For this purpose, various designs have been discussed in the previously published works to enhance the isolation among MIMO antennas.

One of the most common techniques for the enhancement of isolation between MIMO antennas is to design a decoupling network. In [2], a 4-port MIMO antenna was designed for UWB applications. The UWB characteristics were achieved by etching a metamaterial structure from the coplanar waveguide (CPW)–fed rectangular patch element. The results showed that the MIMO antenna offers a bandwidth of 14.58 GHz from 1.8 to 16.38 GHz. To achieve high isolation (> 27.8 dB), a decoupling network consists of four slits and one square slot etched from the common ground of the MIMO structure. In [3], a flexible UWB MIMO antenna was designed where the single radiator was composed of a CPW-fed circular patch. For enhanced isolation, a decoupling structure composed of cross-shaped branches was designed. It was noted that the MIMO antenna configuration offers an isolation of > 22 dB in the frequency range of 2.9–10.86 GHz. The same kind of configuration was presented in [4], where the antenna elements are arranged in a face-to-face configuration. For high isolation (> 15 dB), slots were etched on the ground plane.

In [5], a UWB response was achieved by cutting a circular-shaped monopole antenna into a semicircular shape connected to the stepped microstrip feed line. A stub was placed on each element's ground plane, which acts as a decoupling structure. This configuration leads to an isolation of > 17 dB in the UWB frequency range. The same kind of configuration was used in [6] to achieve UWB characteristics with high isolation. The MIMO radiators consist of a modified rectangular patch and a C-shaped ground that are connected with each other with the help of a decoupling network. In [7], the authors designed a modified semicircular patch radiator–based MIMO antenna for UWB applications. The modification in the semicircular patch was done by etching a guitar-shaped slot. The MIMO antenna was designed by placing the antenna elements in front of each other. A mesh-like decoupling structure was used on the top and back sides of the structure to get high isolation. In [8], a four-element MIMO antenna resembling a stingray fish skeleton was designed for UWB communication systems. For isolation improvement, a window-like decoupling structure was placed between the antenna elements, which tend to achieve > 22 dB isolation among radiating elements. The second possible technique to achieve high isolation is to utilize defected ground structure (DGS). In [9], a design of a fractal patch radiator–based MIMO antenna was presented for UWB applications. The isolation between MIMO radiators was achieved with the help of a square-shaped DGS. In [10], a DGS-based MIMO antenna design was presented for UWB communication systems. The use of a DGS tends to achieve an isolation of > 20 dB in the operating bandwidth.

In the above-reported literature, it is observed that different kinds of decoupling structures are used to achieve high isolation. These kinds of configurations sometimes lead to complex antenna geometries that are difficult to fabricate. In addition, most of the discussed literature focused on the isolation improvement of the MIMO antennas; they did not consider other performance parameters, such as antenna radiation performance that gets lower below expectations. So, there is a need to make a trade-off among MIMO antenna performance parameters. Therefore, in this paper, an effort has been made to design a novel, small, and efficient UWB MIMO antenna. The radiating structure of the MIMO configuration consists of a CPW-fed fractal radiating element that operates from 3.15 to 20 GHz. It is worth saying that an isolation of > 15 dB is achieved between the MIMO radiating elements without the use of any decoupling network, which ensures the self-decoupling property. Moreover, the designed MIMO antenna offers stable radiation characteristics over the entire operating bandwidth. In addition, envelope correlation coefficient (ECC) of < 0.008, total active reflection coefficient (TARC) of > 20 dB, mean effective gain (MEG) of < −3 dB, and CCL below 0.25 bps/Hz are achieved over the operating bandwidth.

2. Polarization Diversity–Based MIMO Antenna

Before explaining the design of the quad-port MIMO antenna, the performance of the single radiating element is presented and discussed in detail.

2.1. Single Fractal Radiating Element. The design of the CPW-fed fractal radiating element is depicted in Figure 1. It is printed on a 1.57-mm-thick low-loss dielectric substrate, namely, Rogers RO5880, with a relative permittivity (ε_r) = 2.2. The antenna design consists of fractal geometry, which is formed by incorporating small circular rings within the main radiator (a circular ring) and a modified CPW ground plane. For the design of the radiating element, the radius of the outer circular ring is determined using the design formulas provided in [11], while the inner circular rings are evenly spaced and rotated by 60°. The change in the ground plane shape is done by truncating the edges in a circular pattern, which helps to achieve wideband multiresonance characteristics, as discussed in [12]. The overall antenna design parameters are L_S = 30, W_S = 25, W_F = 2.8, L_G = 9.2, W_G = 10.65, R_B = 6, D = 19, D_R = 8.4, t = 0.8, and g = 1.2 (all dimensions are in millimeters).

To evaluate the performance of the proposed UWB antenna, CST Microwave Studio v2023 is used. The reflection coefficient ($|S_{11}|$) response of the designed fractal antenna is illustrated in Figure 2(a), and it is observed that it resonates well in the UWB frequency band (3.15–20 GHz). On the other hand, the simulated radiation efficiency and realized gain results are shown in Figure 2(b). The radiation efficiency of the designed antenna is noted to be > 85%, while the gain fluctuates in the range of 1.13–6.13 dBi (see Figure 2(b)).

The radiation patterns of the UWB antenna for both planes (*E*- and *H*-) for different resonant frequencies are depicted in Figure 3. In the *H*-plane, for low-band frequencies, the pattern is omnidirectional (see Figure 3(a)). With the increase in frequency, the *H*-plane pattern becomes quasi-omnidirectional, as shown in Figures 3(b), 3(c), and 3(d). On the other hand, in the *E*-plane, the antenna generates bidirectional patterns for low- and mid-band frequencies, as shown in Figures 3(a), 3(b), and 3(c). As the

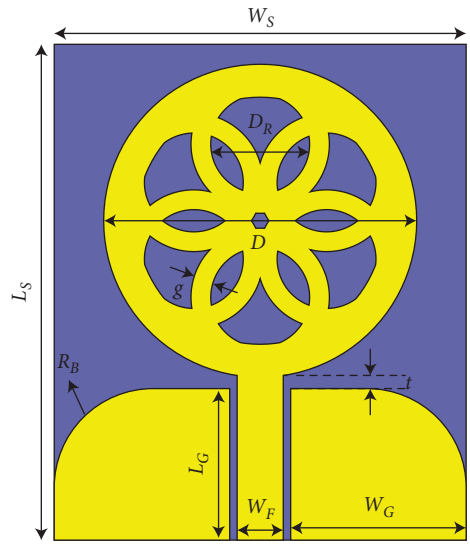

Figure 1: Design of the CPW-fed fractal UWB antenna.

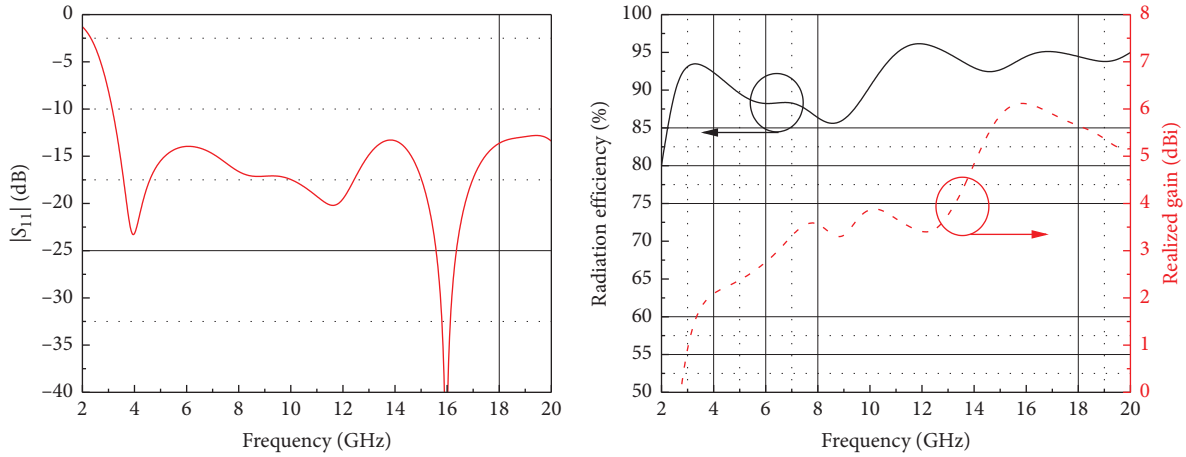

Figure 2: Simulated (a) $|S_{11}|$ and (b) radiation efficiency and realized gain of the CPW-fed fractal UWB antenna.

frequency increases, more nulls are generated in the radiation patterns (see Figure 3(d)), which may be associated with the higher order modes excitation at higher frequencies [12]. To further explain the distortions observed in the *E*-plane radiation patterns, the three-dimensional (3D) radiation patterns of the UWB antenna are plotted and shown in Figure 4. From the 3D patterns, it is observed that they are well aligned with the *E*-plane patterns (see Figure 3, red dashed curve).

It is mentioned above that the ground plane plays a vital role in achieving the UWB response. Therefore, a parametric analysis is conducted by changing the ground plane length L_G from 8 to 10 mm with a step of 0.4 mm. It is observed that as the value of L_G increases (see Figure 5), the impedance matching improves in the operating bandwidth. The wider impedance bandwidth is achieved when the L_G value reaches up to 9.2 mm. After that, the matching becomes worse at lower frequency bands, as shown in Figure 5.

In addition to the frequency-domain analysis, it is essential to evaluate the time-domain performance of the UWB antenna. For the analysis, two antenna elements are arranged in a transceiver mode apart from each other at a distance of 15 cm. The performance is evaluated for two configurations, i.e., side-by-side (SbS) and face-to-face (F2F) configurations. For the excitation of the antennas, a Gaussian pulse is generated, whose operating range is from 1 to 20 GHz. This analysis will tell how much the pulse was distorted when it reached the receiver side. Figure 6(a) shows the normalized pulse response for both configurations, and it can be noted that the UWB antenna is able to receive the signals with low distortions. This phenomenon is also verified by checking the fidelity factor for both configurations. For the SbS configuration, the fidelity factor is noted to be 78.60%, while for the F2F configuration, the fidelity factor is equal to 77.42%. In addition to the pulse response, to analyze the phase distortion and dispersion characteristics of

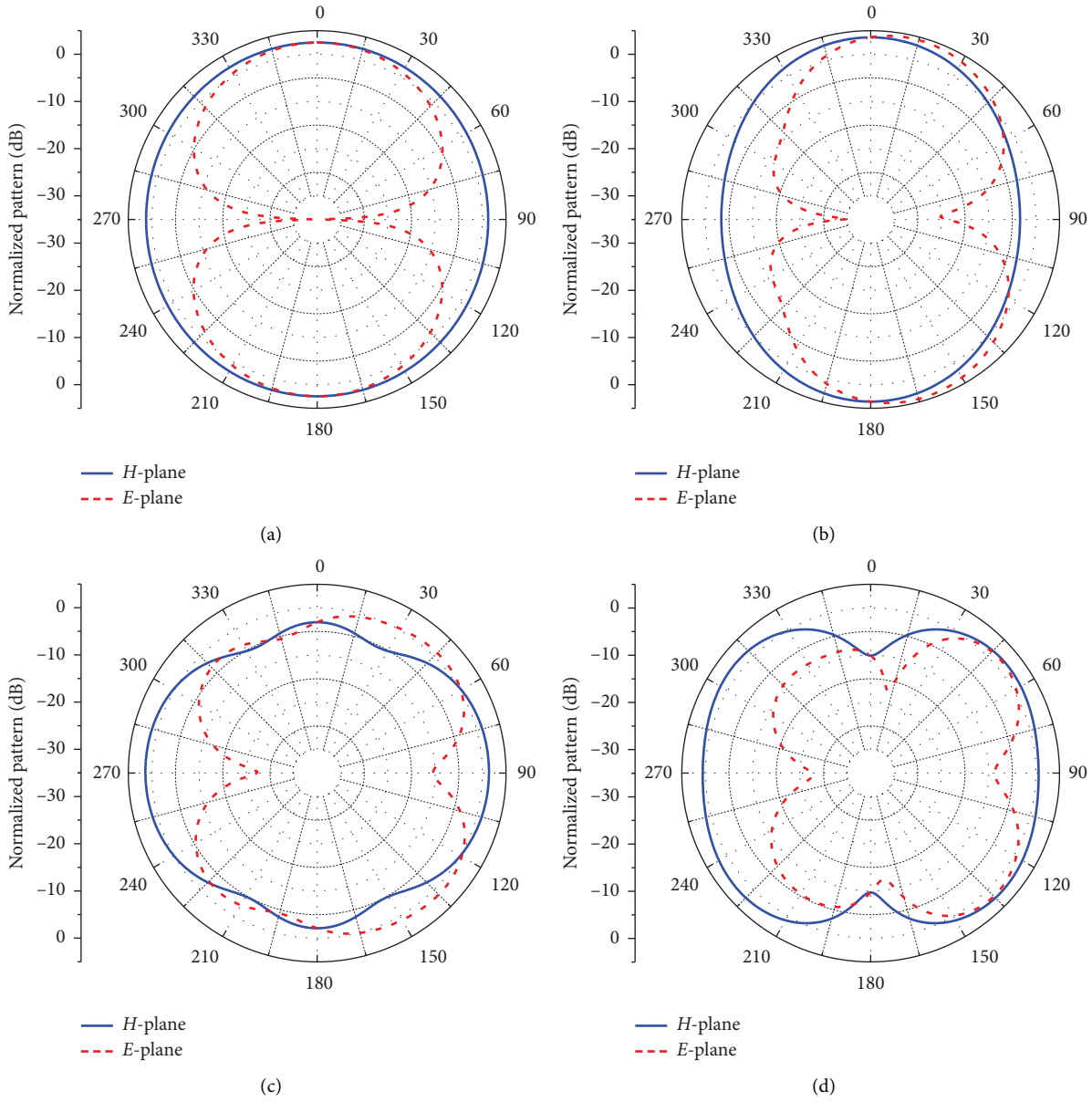

Figure 3: Simulated far-field radiation patterns of the CPW-fed fractal UWB antenna: (a) 4 GHz, (b) 8 GHz, (c) 12 GHz, and (d) 16 GHz.

the UWB antenna, the average delay between the output and the input signal is calculated, which is known as group delay. Figure 6(b) shows the group delay response for both SbS and F2F configurations. Ideally, the group delay should be less than 2 nsec, and for the proposed UWB, a group delay of less than 1 nsec is noted for both configurations.

2.2. Four-Port MIMO Antenna Configuration. After discussing the performance of the single antenna element, the design of the proposed polarization-diversity–based MIMO antenna configuration is presented, as shown in Figure 7(a), while the fabricated prototype is shown in Figure 7(b). To obtain polarization diversity, four antenna elements are arranged in an orthogonal manner. The dimensions of the single MIMO radiator are the same, as shown in Figure 1. One can observe from Figure 7(a) that the fractal radiating elements are arranged close to each other, which leads to a compact size with dimensions of $W_M \times L_M = 55 \times 55\ \text{mm}^2$.

The equivalent lumped components' circuit model of the proposed MIMO antenna is shown in Figure 8(a). The circuit is modeled by connecting three parallel RLC resonant circuits (considering the resonant frequencies in the operating bandwidth) in series to cover the desired operating bandwidth. The input port resistance (R_0), self-probe inductance (L_0), and the static antenna capacitance (C_0) are placed serially with the parallel RLC resonant circuits. In the circuit model, R_k, L_k, and C_k represent resistance, inductance, and capacitance, respectively, of each resonant section. Based on the equivalent circuit model, the antenna impedance (Z_a) can be calculated as follows:

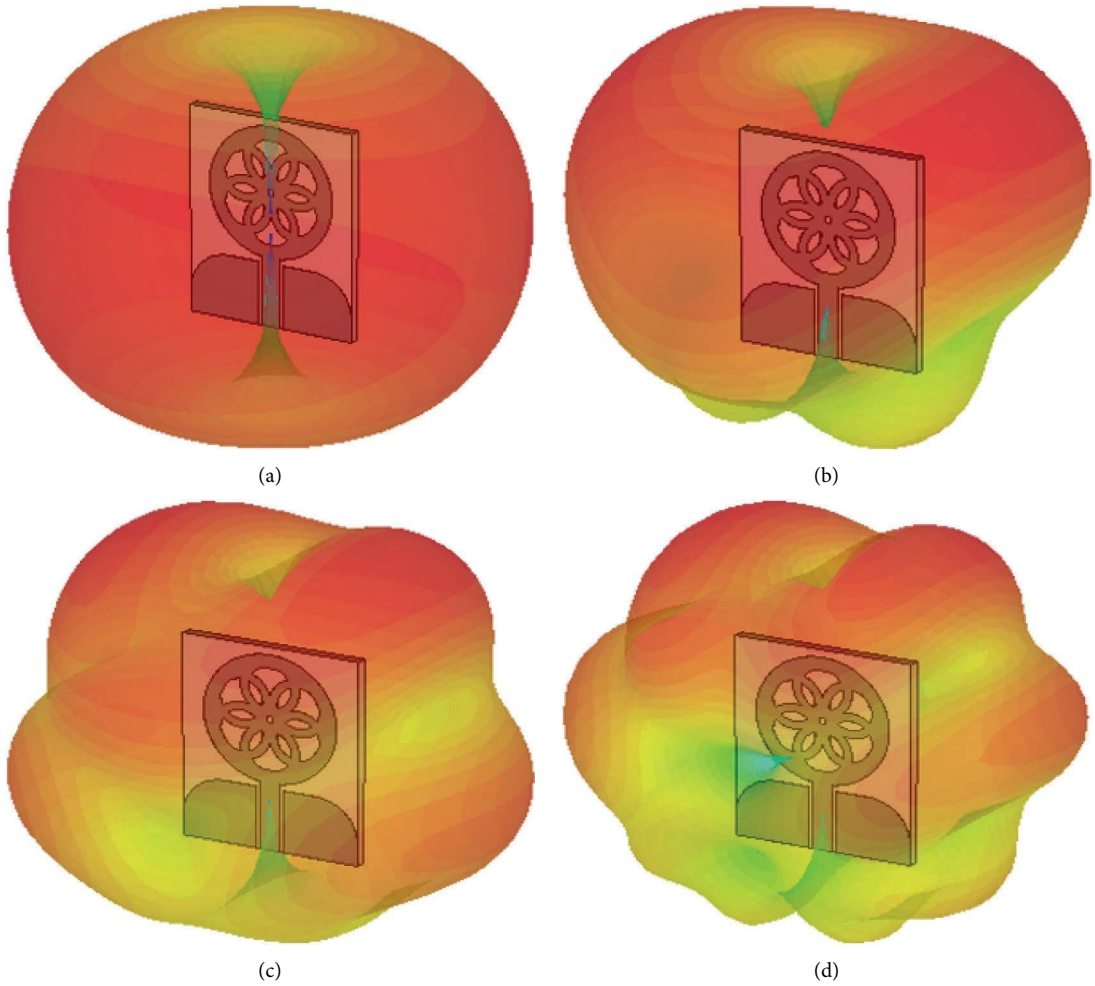

Figure 4: Simulated 3D radiation patterns of the CPW-fed fractal UWB antenna: (a) 4 GHz, (b) 8 GHz, (c) 12 GHz, and (d) 16 GHz.

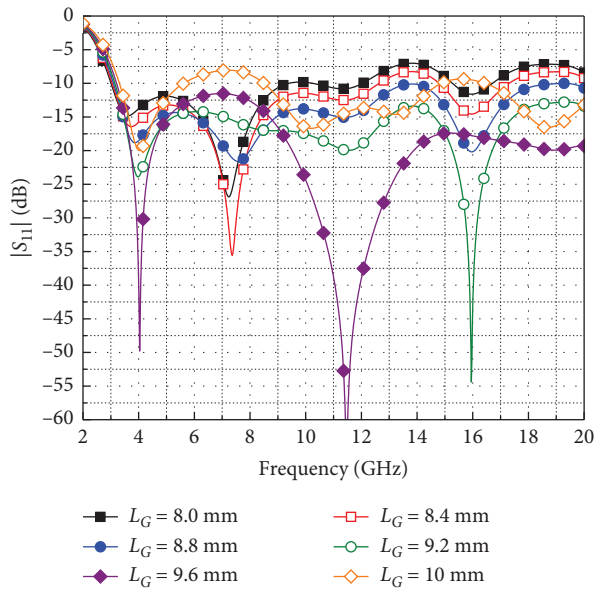

Figure 5: The effect of parameter L_G on antenna's $|S_{11}|$.

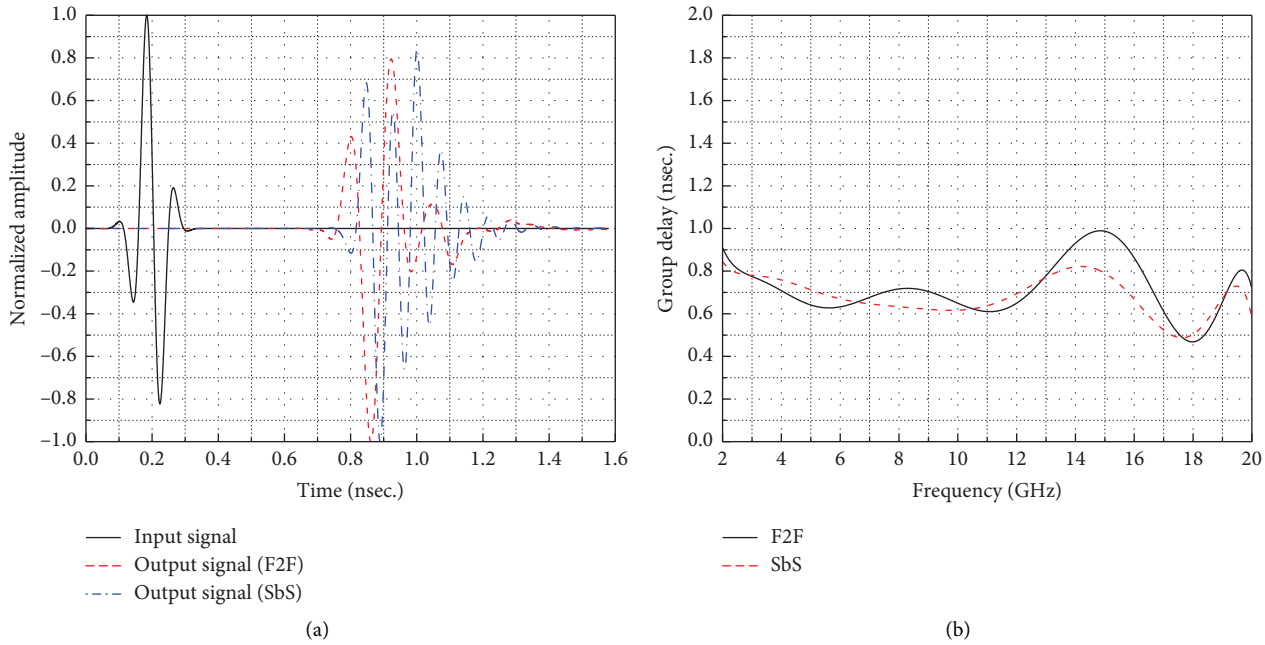

Figure 6: (a) Input and output signals for F2F and SbS configurations. (b) Group delay versus frequency response of the proposed CPW-fed fractal UWB antenna.

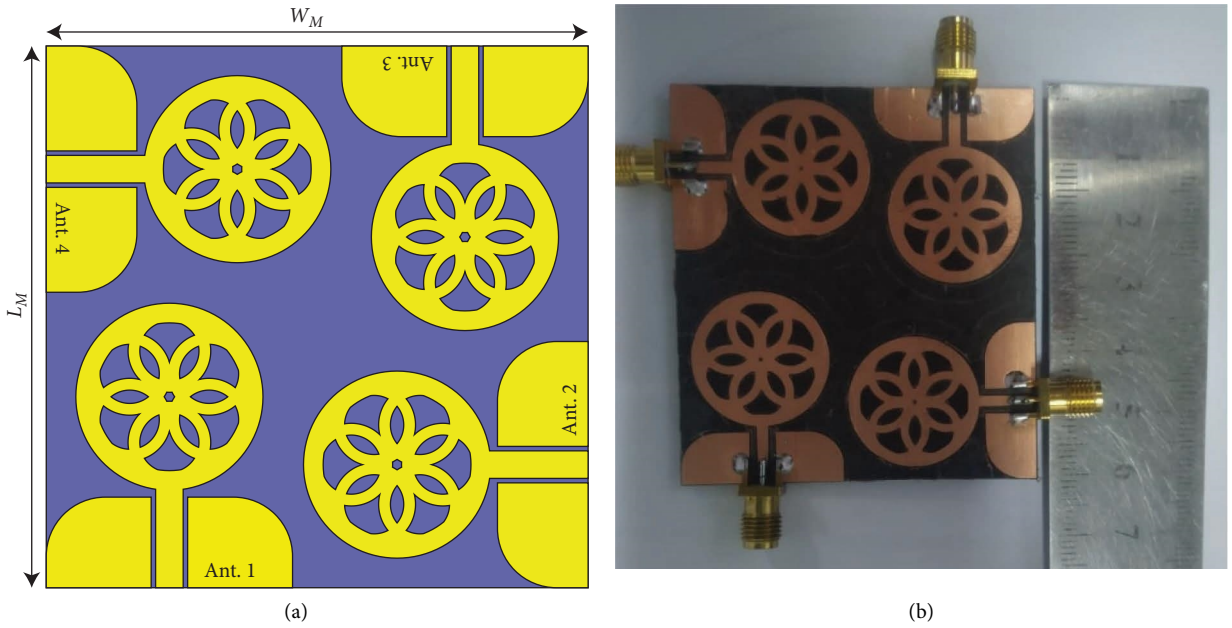

Figure 7: (a) Configuration and (b) fabricated prototype of the four-port CPW-fed fractal UWB MIMO antenna.

$$Z_a = \left(j \times \frac{\omega^2 L_0 C_0 - 1}{\omega C_0}\right) + \left(\sum_{k=1}^{m} \frac{j\omega R_k L_k}{R_k\left(1 - \omega^2 L_k C_k\right) + \left(j\omega L_k\right)}\right), \tag{1}$$

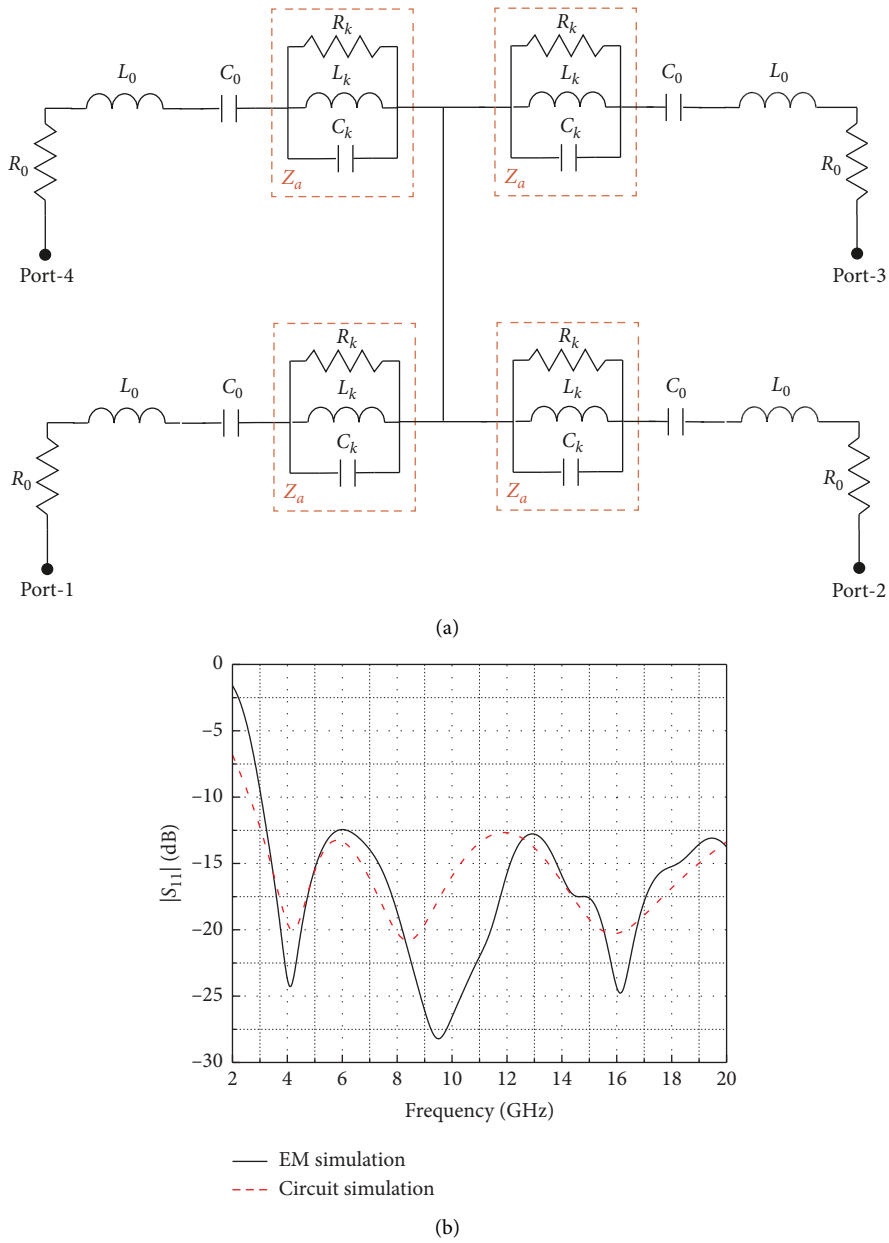

Figure 8: (a) Equivalent circuit model of the CPW-fed fractal UWB MIMO antenna. (b) Comparison between simulated and equivalent circuit $|S_{11}|$ characteristics.

where ω is the angular resonant frequency, $m = 3$, and k represent the number of resonant RLC branches. The designed circuit model is simulated, and the component values are optimized in the advanced design system (ADS) simulation software. The optimum values of the circuit components are $R_0 = 50\,\Omega$, $L_0 = 0.256\,\text{nH}$, $C_0 = 0.0013\,\text{nF}$, $R_1 = 35\,\Omega$, $L_1 = 0.0186\,\text{nH}$, $C_1 = 0.00182\,\text{nF}$, $R_2 = 25.5\,\Omega$, $L_2 = 0.307\,\text{nH}$, $C_2 = 0.00258\,\text{nF}$, $R_3 = 27.3\,\Omega$, $L_3 = 0.121\,\text{nH}$, and $C_3 = 0.0014\text{nF}$. The comparison between $|S_{11}|$ response of the equivalent circuit model and CST simulations is shown in Figure 8(b). It can be observed that the equivalent circuit model response matched well with the simulated data.

The simulated and measured reflection coefficients of the proposed MIMO antenna are illustrated in Figure 9(a). The reflection coefficients are measured using a precision network analyzer (PNA) E8363C in the frequency range of 1–20 GHz. Due to symmetry, the reflection coefficients of Antennas 1 and 2 are presented. One can observe from the result of Figure 9(a) that both the reflection coefficient curves (simulated and measured) are matching well. It can also be noted that the MIMO antenna elements resonate well from 3.15 to 20 GHz. The simulated and measured isolation characteristics of the MIMO antenna are shown in Figure 9(b). In MIMO antennas, there should be high isolation between the radiating elements, which is crucial for

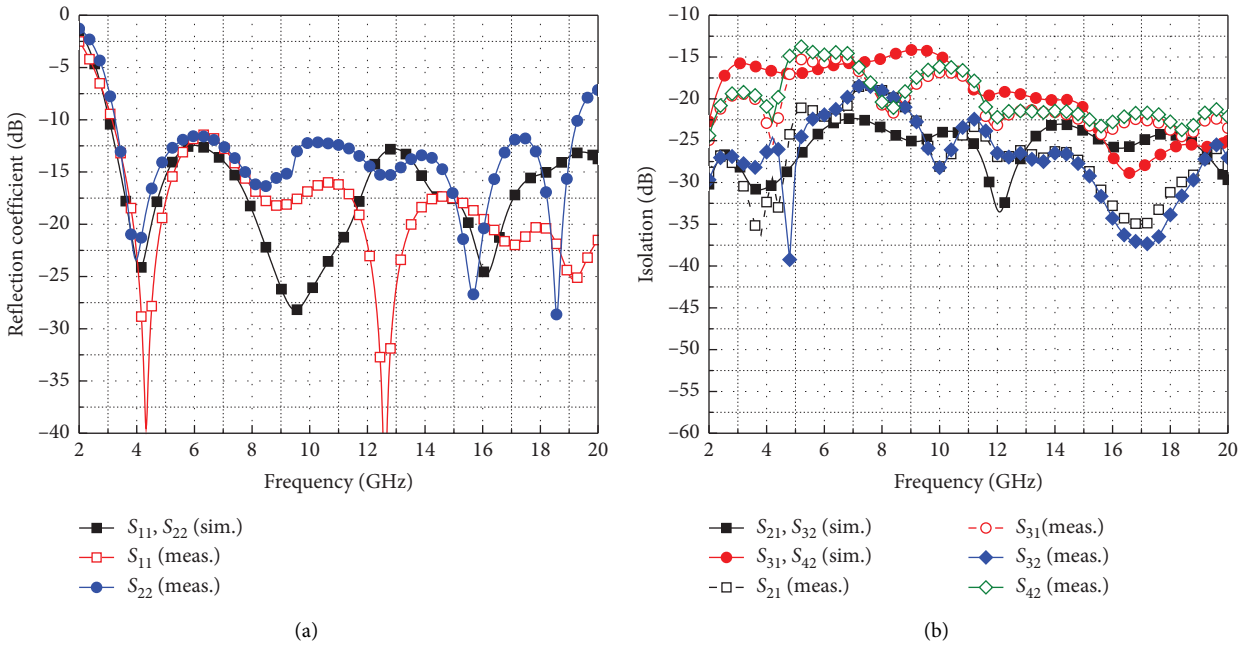

Figure 9: (a) Reflection coefficient and (b) isolation performance of the CPW-fed fractal UWB MIMO antenna.

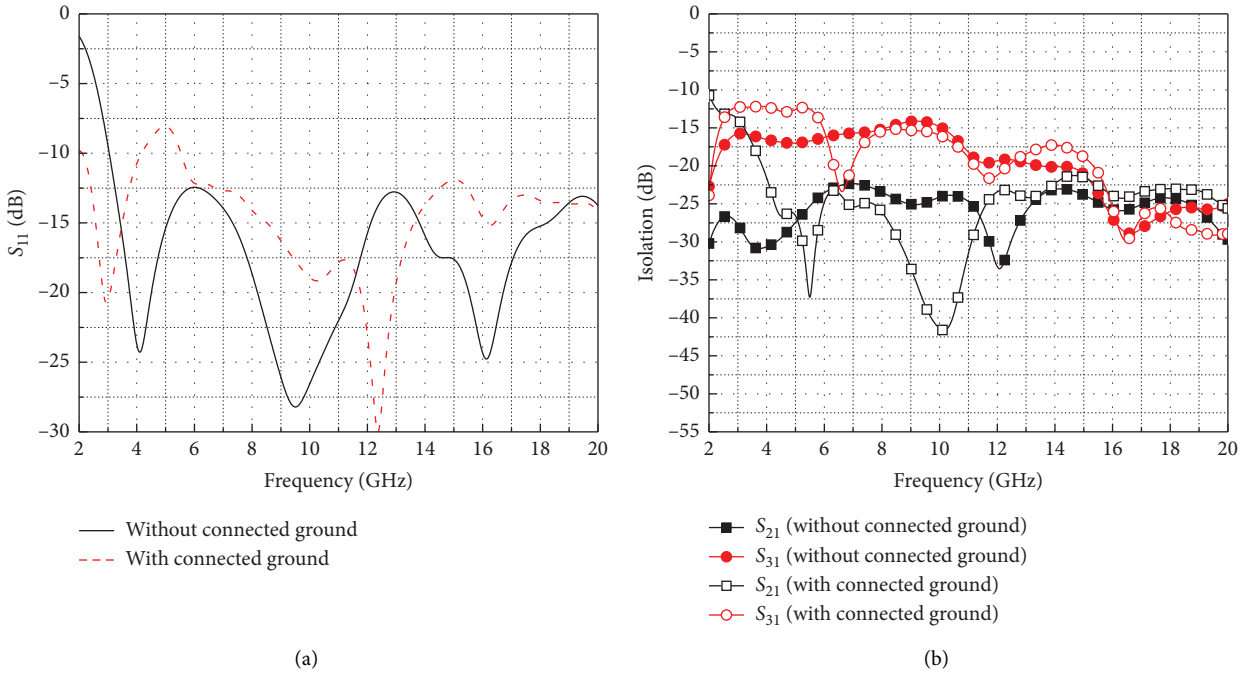

Figure 10: Simulated (a) reflection coefficient and (b) isolation performance of the CPW-fed fractal UWB MIMO antenna without and with connected ground configuration.

maintaining the independence of each antenna's signal path, which is essential for achieving the desired diversity and multiplexing gains. High isolation between radiating elements also reduces interference and crosstalk, thereby improving the overall system performance, enhancing data throughput, and ensuring reliable communication in MIMO systems. From Figure 9(b), it can be seen that the proposed MIMO configuration offers an isolation of > 15 dB between radiating elements over the entire operating bandwidth. The minor differences between the measured and simulated data can be attributed to SMA connector losses and manufacturing tolerances.

For practical applications, it is necessary that the MIMO antenna system should be connected to the device ground plane to avoid unnecessary complexities. Therefore, an analysis is conducted where the MIMO antenna ground

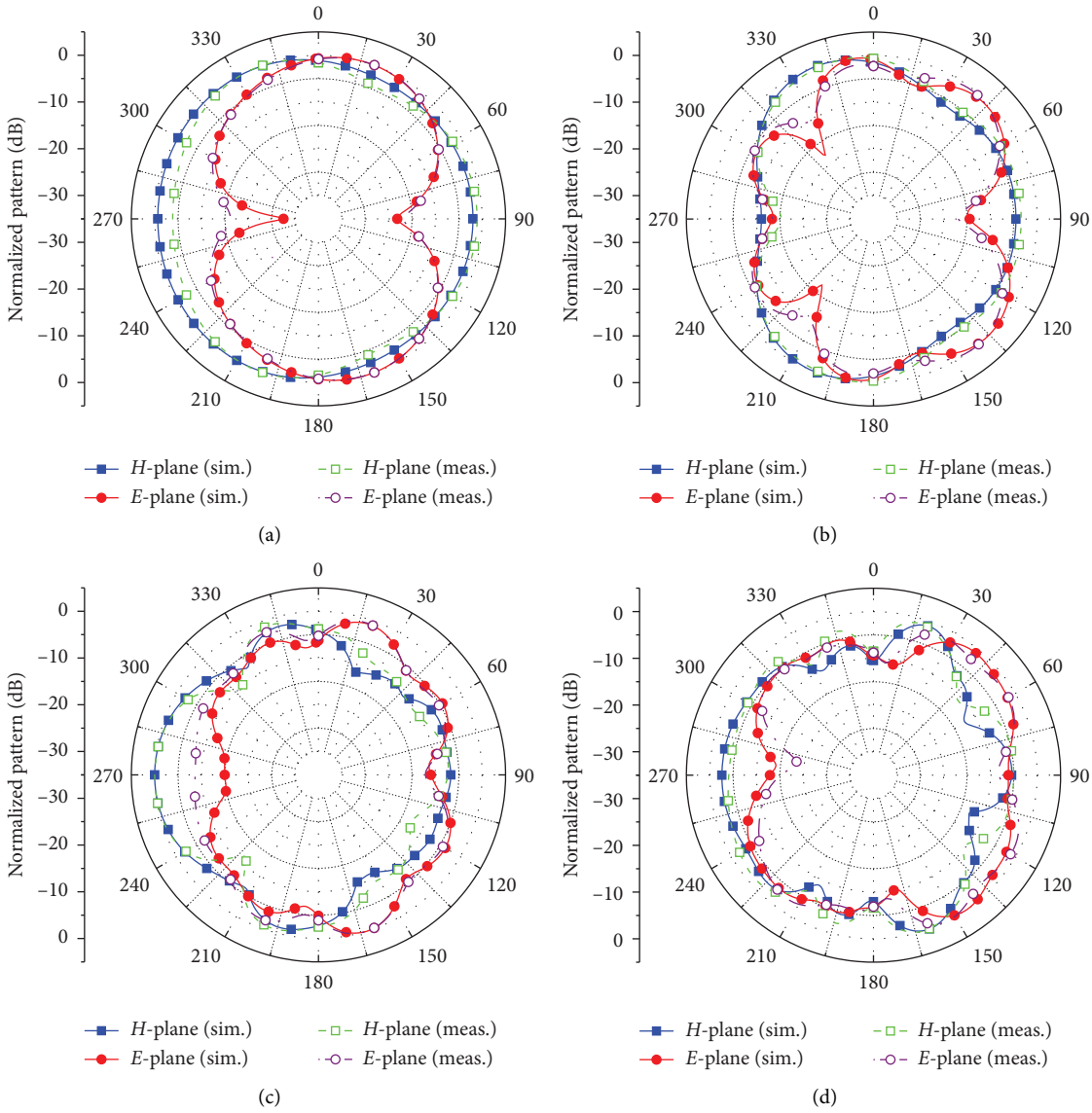

Figure 11: Far-field radiation patterns of Antenna 1 of the CPW-fed fractal UWB MIMO antenna: (a) 4 GHz, (b) 8 GHz, (c) 12 GHz, and (d) 16 GHz.

planes are connected to each other, and the results are shown in Figure 10. From Figure 10(a), one can note that the proposed MIMO antenna works well with the connected ground configuration. A minor impedance mismatch is observed between 4 and 6 GHz, which could be associated with the surface current interaction of MIMO antenna elements. Furthermore, from the isolation plot (see Figure 10(b)), it is observed that for connected ground configuration, the isolation between adjacent antenna elements is less than 15 dB, and for diagonally placed elements, the isolation value is less than 12 dB, which aligns well with the minimum required isolation value. Based on the results, one can say that the proposed MIMO antenna has the ability to perform well even in connected ground configuration.

The simulated and measured far-field radiation patterns of the proposed MIMO antenna for both *E*- and *H*-planes are shown in Figures 11 and 12. To verify the polarization diversity, the radiation patterns are characterized only for two antenna elements, i.e., Antenna 1 and Antenna 2, for different frequencies. For lower frequency bands (4 and 8 GHz), as shown in Figures 11(a) and 11(b), Antenna 1 exhibits bidirectional patterns in the *E*-plane. For the *H*-plane, the pattern is omnidirectional at 4 GHz and quasi-omnidirectional at 8 GHz. As the frequency increases (> 8 GHz), the pattern becomes quasi-omnidirectional with some distortions in both planes, as shown in Figures 11(c) and 11(d). Furthermore, in a polarization diversity configuration, the antenna elements are arranged orthogonally; therefore, the radiation characteristics should be the same. The only difference is that the *E*-plane pattern of Antenna 1 is equal to the *H*-plane pattern of Antenna 2, and vice versa [13]. This kind of behavior can be noted from the plots in Figure 12, where the radiation patterns of Antenna 2 are plotted.

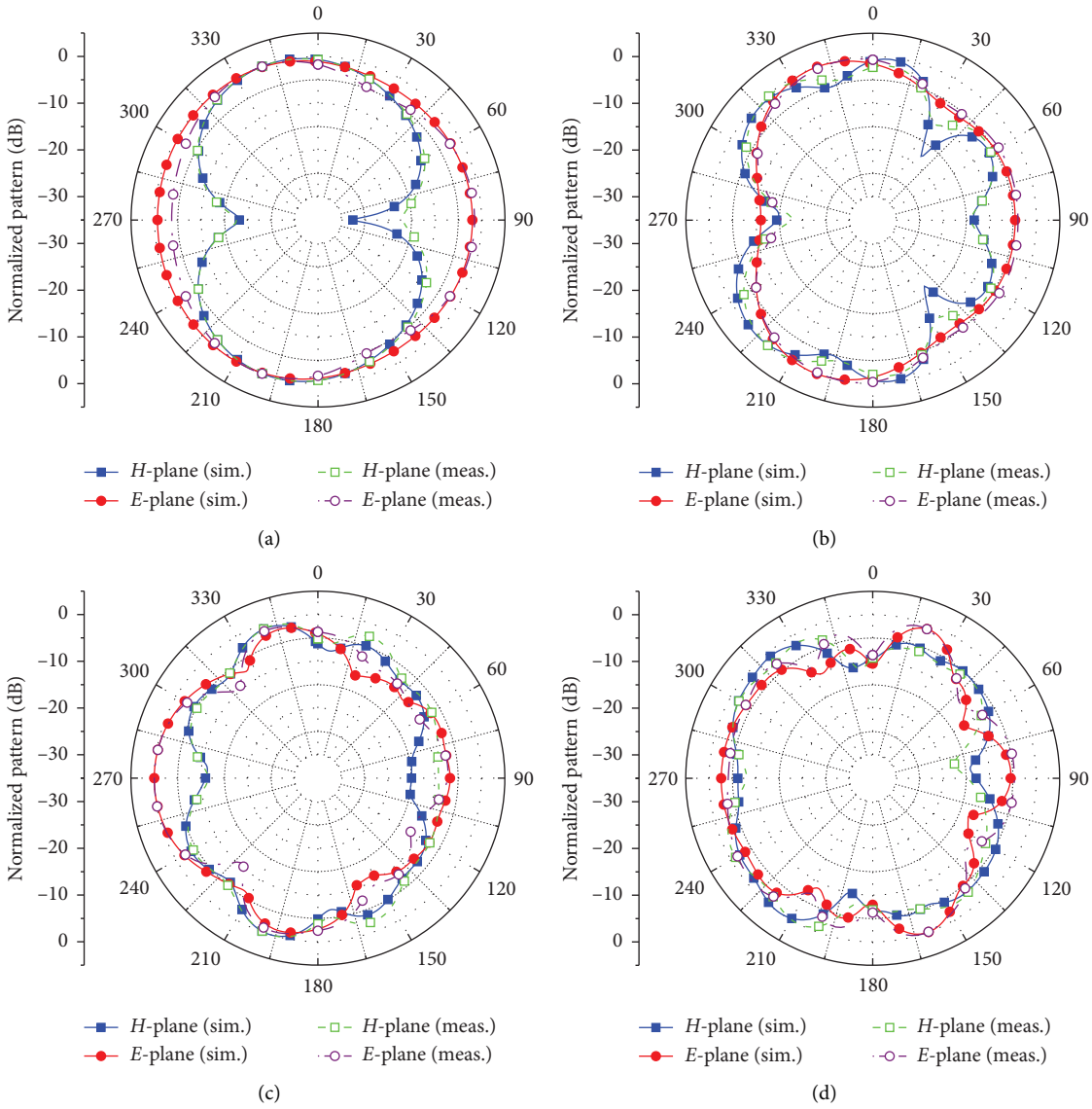

Figure 12: Far-field radiation patterns of Antenna 2 of the CPW-fed fractal UWB MIMO antenna: (a) 4 GHz, (b) 8 GHz, (c) 12 GHz, and (d) 16 GHz.

2.2.1. MIMO Performance Parameters. When designing MIMO antennas, it is essential to evaluate MIMO system performance parameters, such as ECC, MEG, TARC, and CCL. ECC measures the correlation between signals from different antenna elements, where lower ECC values (< 0.5) indicate greater independence and better spatial diversity, which is ideal for maximizing MIMO system efficiency, while ECC < 1 is less optimal. ECC can be calculated using the far-field radiation characteristics of the designed MIMO antenna system as follows [13–15]:

$$ECC = \frac{\left|\int_0^{2\pi}\int_0^{\pi}\left[M_1(\theta,\phi).M_2^*(\theta,\phi)\right]\sin\theta d\theta\, d\phi\right|^2}{\left(\int_0^{2\pi}\int_0^{\pi}\left|M_1(\theta,\phi)\right|^2\sin\theta d\theta\, d\phi\right)\left(\int_0^{2\pi}\int_0^{\pi}\left|M_2(\theta,\phi)\right|^2\sin\theta d\theta\, d\phi\right)}, \quad (2)$$

where $M_1(\theta,\phi)$ and $M_2(\theta,\phi)$ are the far-field radiation patterns of the two antennas, and θ and ϕ are the elevation and azimuth angles, respectively.

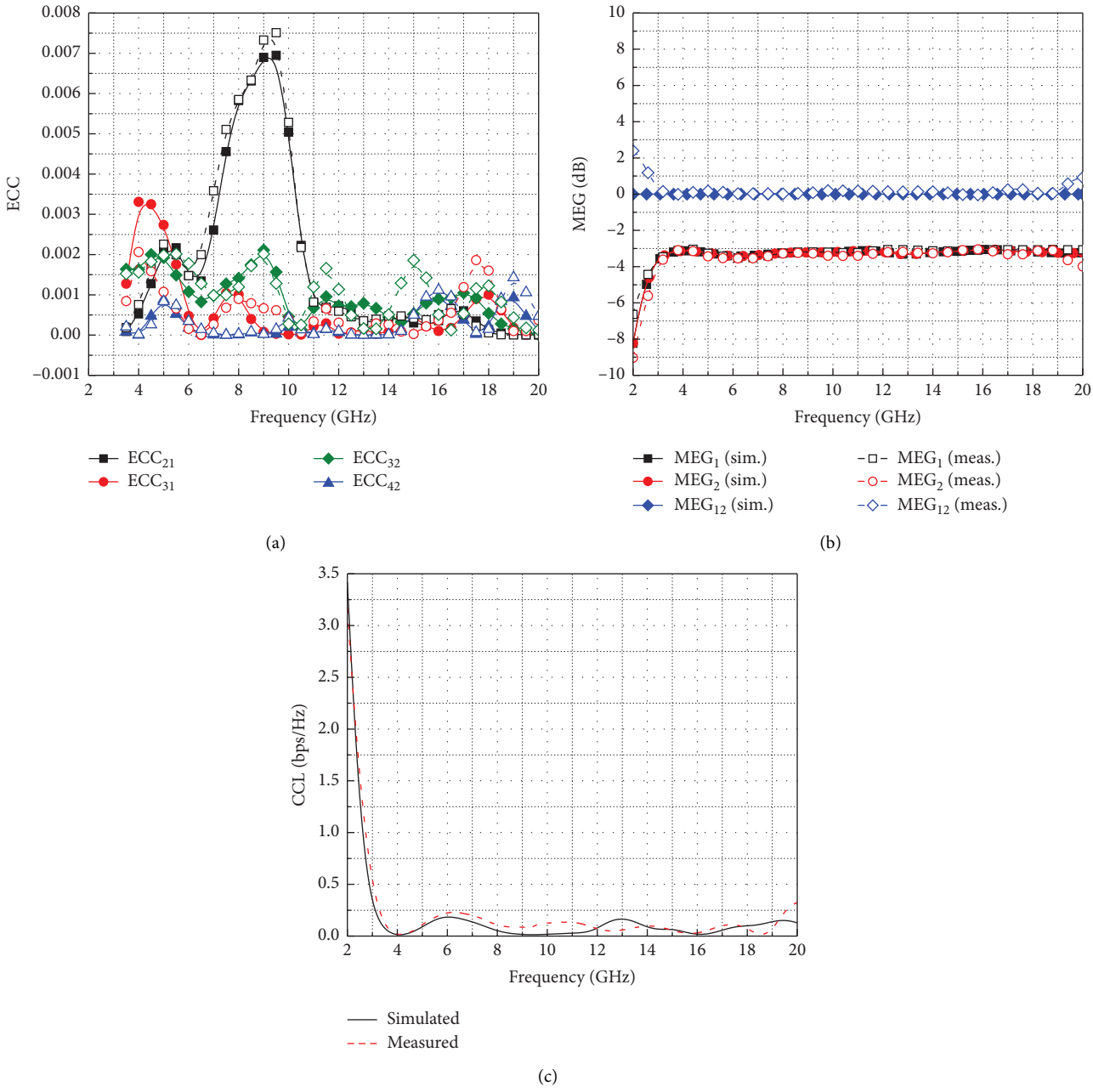

Figure 13: (a) ECC, (b) MEG, and (c) CCL of the CPW-fed fractal UWB MIMO antenna. In the ECC plot, the solid line shows simulated data, while the dashed (--) line shows measurement data.

The comparison between simulated and measured ECC is shown in Figure 13(a). It is observed that for the entire frequency band, the simulated and measured ECC values are less than 0.008.

The second important parameter evaluated to assess the MIMO antenna performance is MEG. It shows the measurement of the amount of received power by the MIMO radiators compared to an isotropic radiator. For MIMO antennas, one can compute MEG by using S-parameters as follows [15]:

$$\mathrm{MEG}_i = 0.5\left(1 - \sum_{j=1}^{N}\left|S_{ij}\right|^2\right), \quad i = 1, 2, 3, 4. \tag{3}$$

For the proposed MIMO antenna, the MEG is plotted by considering two antenna elements, and the results are plotted in Figure 13(b). It is observed that the value of MEG is less than −3 dB for the operating bandwidth, and it matches well with the practical requirements. In addition, the ratio of both the MEG values is noted to be less than 3 dB, as shown in Figure 13(b).

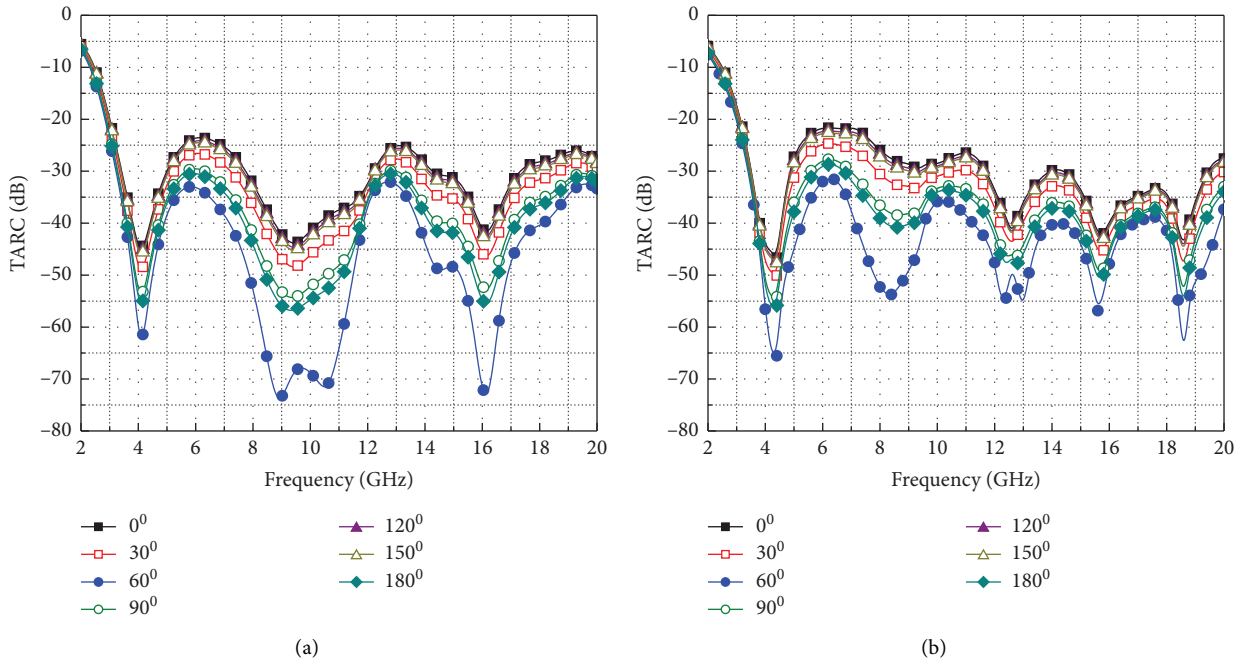

Figure 14: (a) Simulated and (b) measured TARC of the CPW-fed fractal UWB MIMO antenna.

Table 1: Comparison among the proposed UWB MIMO antenna with state-of-the art literature.

References	Ports	Dimensions		Bandwidth (GHz)	Isolation (dB)	Peak gain (dBi)	ECC	CCL (bps/Hz)
		mm^2	λ^2					
[2]	4	51.2 × 51.2	0.17 × 0.17	1–17	> 27.8	7.81	< 0.002	N.A.
[3]	4	65 × 65	0.62 × 0.62	2.9–10.86	> 22	5.5	< 0.01	N.A.
[4]	4	56 × 68	0.72 × 0.88	3.89–17.09	> 15	6.8	< 0.02	< 0.2
[5]	4	45 × 45	0.46 × 0.46	3.1–13.1	> 17	4.0	< 0.02	N.A.
[6]	4	34 × 34	0.34 × 0.34	3–12	> 20	7.2	< 0.35	< 0.34
[7]	4	45 × 45	0.69 × 0.69	4.6–16.4	> 20	8	< 0.002	< 0.2
[8]	4	58 × 58	0.85 × 0.85	4.4–14.4	> 22	3.6	< 0.01	N.A.
[9]	4	40 × 40	0.42 × 0.42	3.2–12.44	> 26	4.9	< 0.0016	< 0.35
[10]	4	40 × 40	0.42 × 0.42	3.2–13.4	> 20	2.0	< 0.005	< 0.1
Prop.	**4**	**55 × 55**	**0.57 × 0.57**	**3.15–20**	**> 15**	**6.13**	**< 0.008**	**< 0.25**

Note: The bold values in the table show the author's presented work.

The third parameter evaluated to assess the MIMO system's performance is CCL, which occurs due to correlation losses. It can be calculated as follows [9]:

$$\mathrm{CCL} = -\log_2 \quad \det\left[\alpha^R\right], \tag{4}$$

where

$$\left[\alpha^R\right] = \begin{bmatrix} \alpha_{11} & \alpha_{12} \\ \alpha_{21} & \alpha_{22} \end{bmatrix}, \tag{5}$$

in which, $\alpha_{11} = 1 - (|S_{11}|^2 + |S_{12}|^2)$, $\alpha_{12} = -(S_{11}S_{12} + S_{21}S_{12})$, $\alpha_{21} = -(S_{22}S_{21} + S_{12}S_{21})$, and $\alpha_{22} = 1 - (|S_{22}|^2 + |S_{21}|^2)$. For the proposed MIMO antenna configuration, CCL is calculated between two antennas, and it is observed that both the simulated and measured CCL are less than acceptable ranges (< 0.5 bps/Hz), as shown in Figure 13(c).

To efficiently characterize the operating bandwidth of the MIMO antenna system, the analysis of S-parameters is not enough. Therefore, TARC is used for the bandwidth characterization of the MIMO antenna, and it can be expressed using the S-parameters of the MIMO antenna as follows [16]:

$$\mathrm{TARC} = \sqrt{\frac{\left(\left|S_{aa} + S_{ab}e^{j\theta}\right|\right)^2 \left(\left|S_{ba} + S_{bb}e^{j\theta}\right|\right)^2}{2}}, \tag{6}$$

where S_{aa} and S_{bb} are the reflection coefficients, S_{ab} and S_{ba} represent transmission coefficients between Port a and b, and θ is the input wave phase. To calculate the TARC, the value of θ is changed from 0° to 180° with a step of 30°. In addition, two MIMO antenna elements are considered to evaluate TARC, and the results are shown in Figure 14. From

both simulated and measured plots, it is noted that the TARC value is well below −20 dB, which satisfies stable performance in the entire operating bandwidth.

Table 1 shows a comparison between designed and previously reported UWB MIMO antennas. Although the physical dimensions of the proposed antenna are large compared to the designs presented in [2, 5–7, 9, 10], it offers a higher impedance bandwidth compared to the previously presented designs. Furthermore, from the gain values, it is observed that the single MIMO element offers high gain compared to the designs presented in [3, 5, 8–10]. In terms of the MIMO performance parameters, the isolation performance of the proposed MIMO antenna is in an acceptable range; it offers low ECC compared to the designs of [3–6, 8].

3. Conclusions

This study presents the design of a novel fractal antenna for UWB MIMO applications. It is observed from the presented results that the designed fractal antenna, with the help of a modified CPW-feed structure, offers a wide impedance bandwidth from 3.15 to 20 GHz. To utilize the proposed UWB antenna design for MIMO communication systems, a polarization-diversity–based MIMO antenna configuration is designed. From both simulated and measured performance, it is noted that the isolation of > 15 dB is achieved between radiating elements without the use of any decoupling network. In addition, the single radiating element of the MIMO antenna system offers a peak realized gain of 6.13 dBi and a radiation efficiency > 85%. The MIMO key performance parameters, such as ECC, MEG, CCL, and TARC, were evaluated and found to be within satisfactory limits, confirming the reliability and effectiveness of the proposed design for UWB MIMO applications.

Data Availability Statement

The data that support the findings of this study are available from the corresponding authors upon reasonable request.

Conflicts of Interest

The authors declare no conflicts of interest.

Funding

This work was supported by the Fundamental Research Funds for the Central Universities under Grant No. 4006002302.

Acknowledgments

The authors would like to thank the Fundamental Research Funds for the Central Universities (Grant No. 4006002302) for providing funding for this research work.

References

[1] Z. Li, X. Zhu, and C. Yin, "CPW-Fed Ultra-wideband Slot Antenna with Broadband Dual Circular Polarization," *AEU-International Journal of Electronics and Communications* 98 (2019): 191–198, https://doi.org/10.1016/j.aeue.2018.11.018.

[2] Z. He and J. Jin, "Compact Quad-Port MIMO Antenna With Ultra-wideband and High Isolation," *Electronics* 11, no. 20 (2022): 3408, https://doi.org/10.3390/electronics11203408.

[3] J. Zhang, C. Du, and R. Wang, "Design of a Four-Port Flexible UWB-MIMO Antenna with High Isolation for Wearable and IoT Applications," *Micromachines* 13, no. 12 (2022): 2141, https://doi.org/10.3390/mi13122141.

[4] A. Desai, J. Kulkarni, M. M. Kamruzzaman, Š. Hubálovský, H.-T. Hsu, and A. A. Ibrahim, "Interconnected CPW Fed Flexible 4-port MIMO Antenna for UWB, X, and Ku Band Applications," *IEEE Access* 10 (2022): 57641–57654, https://doi.org/10.1109/access.2022.3179005.

[5] A. Wu, M. Zhao, P. Zhang, and Z. Zhang, "A Compact Four-Port MIMO Antenna for UWB Applications," *Sensors* 22, no. 15 (2022): 5788, https://doi.org/10.3390/s22155788.

[6] P. P. Shome, T. Khan, A. A. Kishk, and Y. M. M. Antar, "Quad-element MIMO Antenna System Using Half-Cut Miniaturized UWB Antenna for IoT-Based Smart Home Digital Entertainment Network," *IEEE Internet of Things Journal* 10, no. 20 (2023): 17964–17976, https://doi.org/10.1109/jiot.2023.3280628.

[7] P. Kumar, S. Pathan, S. Vincent, et al., "A Compact Quad-Port UWB MIMO Antenna With Improved Isolation Using a Novel Mesh-like Decoupling Structure and Unique DGS," *IEEE Transactions on Circuits and Systems II: Express Briefs* 70, no. 3 (2023): 949–953, https://doi.org/10.1109/tcsii.2022.3220542.

[8] H. Ş. Savcı, "A Four Element Stringray-Shaped MIMO Antenna System for UWB Applications," *Micromachines* 14, no. 10 (2023): 1944, https://doi.org/10.3390/mi14101944.

[9] A. C. Suresh, T. S. Reddy, B. T. P. Madhav, et al., "A Novel Design of Spike-Shaped Miniaturized 4 × 4 MIMO Antenna for Wireless UWB Network Applications Using Characteristic Mode Analysis," *Micromachines* 14, no. 3 (2023): 612, https://doi.org/10.3390/mi14030612.

[10] K. Pandya, T. Upadhyaya, U. Patel, et al., "Performance Analysis of Quad-Port UWB MIMO Antenna System for Sub-6 GHz 5G, WLAN and X Band Communications," *Results in Engineering* 22 (2024): 102318, https://doi.org/10.1016/j.rineng.2024.102318.

[11] K. P. Ray, "Design Aspects of Printed Monopole Antennas for Ultra-wide Band Applications," *International Journal of Antennas and Propagation* 2008 (2008): 1–8, https://doi.org/10.1155/2008/713858.

[12] U. Rafique, M. M. Ahmed, M. M. Hassan, and H. Khalil, "A Modified Super-wideband Planar Elliptical Monopole Antenna," in *2018 Progress in Electromagnetics Research Symposium (PIERS-Toyama)* (IEEE, 2018), 2344–2349.

[13] M. N. Zahid, Z. Gaofeng, S. H. Kiani, et al., "H-Shaped Eight-Element Dual-Band MIMO Antenna for Sub-6 GHz 5G Smartphone Applications," *IEEE Access* 10 (2022): 85619–85629, https://doi.org/10.1109/access.2022.3189658.

[14] A. G. Alharbi, U. Rafique, S. Ullah, et al., "Novel MIMO Antenna System for Ultra-wideband Applications," *Applied*

Sciences 12, no. 7 (2022): 3684, https://doi.org/10.3390/app12073684.

[15] S. Agarwal, U. Rafique, R. Ullah, S. Ullah, S. Khan, and M. Donelli, "Double Overt-Leaf Shaped CPW-Fed Four Port UWB MIMO Antenna," *Electronics* 10, no. 24 (2021): 3140, https://doi.org/10.3390/electronics10243140.

[16] G. Rajesh and R. Poonkuzhali, "Design and Analysis of CPW Fed Ultrathin Flexible MIMO Antenna for UWB and X-Band Applications," *IEEE Access* 12 (2024): 96704–96717, https://doi.org/10.1109/access.2024.3426592.